Electrochimica Acta 201 (2016) 279–285

Contents lists available at ScienceDirect

Electrochimica Acta

journal homepage: www.elsevier.com/locate/electacta

Evaluation and Enhancement of the Oxygen Reduction Reaction Activity on Hafnium Oxide Nanoparticles Assisted by L(+)-lysine

Mitsuharu Chisaka*, Noriaki Itagaki

Department of Electronics and Information Technology, Hirosaki University, 3 Bunkyo-cho, Hirosaki, Aomori 036-8561, Japan

ARTICLE INFO

Article history:
Received 11 August 2015
Received in revised form 29 October 2015
Accepted 29 October 2015
Available online 2 November 2015

Keywords:
hafnia
carbothermal reduction
catalyst
cathode
polymer electrolyte fuel cell

ABSTRACT

Evaluation of the oxygen reduction reaction (ORR) on oxide compounds is difficult owing to the insulating nature of oxides. In this study, various amounts of L(+)-lysine were added to the precursor dispersion for the hydrothermal synthesis of hafnium oxide nanoparticles on reduced graphene oxide sheets (HfO_x–rGO) to coat the HfO_x catalysts with layers of carbon, thereby increasing the conductivity and number of active sites. When the mass ratio of L(+)-lysine to GO, *R*, was above 26, carbon layers were formed and the amount monotonically increased with increasing *R*, as noted by cyclic voltammogrametry. X-ray photoelectron spectroscopy and rotating disk electrode analyses revealed that pyrolysis produced ORR-active oxygen defects, whose formation was proposed to involve carbothermal reduction. When $53 \leq R \leq 210$, HfO_x–rGO contained a similar amount of oxygen defects and ORR activity, as represented by an onset potential of 0.9 V versus the reversible hydrogen electrode in 0.1 mol dm^{-3} H_2SO_4. However, the number of active sites depended on *R* due to the amount of L(+)-lysine-derived carbon layers that increased both the number of active sites and resistivity towards oxygen diffusion.

1. Introduction

The electrocatalytic reduction of oxygen has garnered significant attention owing to the need for cathodes in energy conversion devices for use in a variety of applications. Typical examples include Zn-air batteries in hearing aids, Al-air and Mg-air batteries in underwater propulsion devices, alkaline fuel cells (AFCs) in space craft, and polymer electrolyte fuel cells (PEFCs) in compact portable devices, stationary power systems, and vehicles. The electrolyte used in most of these energy conversion devices is alkaline media, where the oxygen reduction reaction (ORR) proceeds more smoothly than in acidic counterparts; therefore, the cathodes do not necessarily require catalysts based on platinum group metals (PGMs). PEFCs that utilize acidic polymer electrolyte membranes are of particular interest owing to the economic impact of the potential applications; however, the cathode requires excessive amounts of PGM catalysts for widespread use [1]. Therefore, extensive efforts have been made towards the development of non-PGM catalysts in acidic media [2–20].

The number of non-PGM catalysts for use in PEFC cathodes is limited owing to the corrosive conditions; the pH value is estimated to be equal to or less than 1 [2], in addition to the high operating potential, e.g., 0.6–1.0 V versus the reversible hydrogen electrode, in vehicles. Most of the recent works on non-PGM catalysts have focused on nitrogen-doped graphitic carbon materials synthesized in the absence [3–6] and presence of iron/cobalt sources [2,7–12]. This type of catalyst has been synthesized via various routes and can show high ORR activity in acidic media when the graphitic layer is disordered by nitrogen doping to expose a large number of edges. Some of the activities are comparable to that of platinum, although the durability is often insufficient [12].

We have focused on another type of non-PGM catalyst, namely oxide compounds containing group 4/5 metals, owing to the high durability in acidic media confirmed by chemical leaching tests with inductively coupled plasma spectroscopy [13–16]. The drawback of this type of catalyst is the moderate current density, due to the electrical insulation properties. Therefore, recent works have focused on synthesizing oxide/oxynitride nanoparticles on conductive graphitic carbon materials to enlarge the specific surface area [17–20]. We recently developed a new route to synthesize hafnium oxynitride on reduced graphene oxide sheets (HfO_xN_y–rGO) to avoid the use of ammonia gas pyrolysis and to reduce the required catalyst volume by using the rGO sheets [19]. Nonetheless, the “active” surface area should be restricted to the point where the HfO_xN_y nanoparticle catalysts contact the carbon supports. For the accurate evaluation of ORR activity on this

* Corresponding author. Tel.: +81 172 39 3559; fax: +81 172 39 3559.
E-mail address: chisaka@hirosaki-u.ac.jp (M. Chisaka).

http://dx.doi.org/10.1016/j.electacta.2015.10.184
0013-4686/

catalyst, coating the surface with conductive carbon layers that connect catalyst particles with supports are necessary. From this viewpoint, the decomposition of oxy-tantalum phthalocyanine was recently used to produce carbon layers that connected nano-tantalum oxide catalysts with multi-walled carbon nanotube supports [20]. However, the use of phthalocyanine-based polymers inevitably increases the cost of the catalyst and the carbon content of the resulting catalyst cannot be controlled because the molar ratio of tantalum to carbon is fixed in the oxy-tantalum phthalocyanine precursor. Therefore, an alternative metal-free carbon source is necessary.

In this study, L(+)-lysine was used as a carbon source to connect nitrogen-free HfO_x catalysts with rGO sheets. L(+)-lysine was selected as Xu et al. succeeded in the hydrothermal synthesis of uniform TiO_2 nanoparticles with the average size of ca. 6 nm and these particles were connected by lysine-derived thin carbon layers. During the hydrothermal synthesis, some nitrogen atoms in L(+)-lysine were doped into the TiO_2 nanoparticles in their study [21] whereas the nitrogen atoms were removed by pyrolysis in order to generate ORR activity via the formation of oxygen defects on HfO_2 in this study. Another role of L(+)-lysine was to increase the pH of the precursor dispersion to hydrolyze the hafnium tetrachloride precursor to hafnium hydroxide, which favored the adsorption of oxygen functional groups on GO to form HfO_2 nanoparticles after pyrolysis [17]. Hafnium is not an inexpensive and abundant element: the price in 2010 is $563 per kilogram [22] and world reserves of HfO_2 is 660,000 tons, which is only one order of magnitude larger than that of PGMs [23]. However, the present study revealed that the usage could be reduced by increasing the utilization as well as activity. Besides, the developed method for evaluation and enhancement of the ORR activity should be applied to other oxide catalysts, e.g., TiO_2 and ZrO_2. The morphologies, crystal structures, and surface chemical states of the catalysts were systematically investigated using field-emission transmission electron microscopy (FE-TEM), X-ray diffraction (XRD), and X-ray photoelectron spectroscopy (XPS), respectively. The ORR activity and selectivity of the catalysts were also evaluated by rotating disk electrode (RDE) voltammetry and rotating ring-disk electrode (RRDE) voltammetry, respectively.

2. Experimental

2.1. Synthesis of catalysts

20 cm^3 of an aqueous dispersion of GO (2 mg cm^{-3}, 763705, Sigma-Aldrich, U.S.) and 120 cm^3 of distilled water were sonicated for 1 h. The GO dispersion was then poured into a Teflon-lined autoclave under stirring, followed by the addition of 40 cm^3 of ethanol, 0.3 g of $HfCl_4$ (Mitsuwa Chemicals Co., Japan), and various amounts of L(+)-lysine (Wako Pure Chemical Industries, Ltd, Japan) to set the mass ratio of GO:HfO_2:L(+)-lysine to 1:5:*R*, where *R* ranged from 26 to 210. The pH of the resulting dispersion measured by pH test paper was always greater than 10. Next, the autoclave was closed then set in an aluminum block which was placed on a hot stirrer; hydrothermal treatment commenced at 453 K for 12 h with continuous stirring. After the hydrothermal treatment, the autoclave was allowed to cool and stirring was stopped prior to opening the autoclave. The resulting catalyst particles were washed with distilled water until a neutral pH was obtained. The particles were then dried overnight at 380 K and placed in an alumina boat that was set in a horizontal quartz tube furnace, which was slowly evacuated and purged with N_2 gas. The catalyst samples were heated from room temperature to various temperatures, *T*, at a rate of 10 K min^{-1}. *T* was maintained for 2 h, and the sample was then cooled to room temperature at an uncontrolled rate. The flow rate of N_2 was 100 standard cubic centimeters per minute (sccm; 1 sccm = 1.67×10^{-8} m^3 s^{-1}).

2.2. Characterization

The crystal structures of the catalysts were analyzed using an X-ray diffractometer (M18XHF, Mac Science Co., Japan) with Cu-Kα

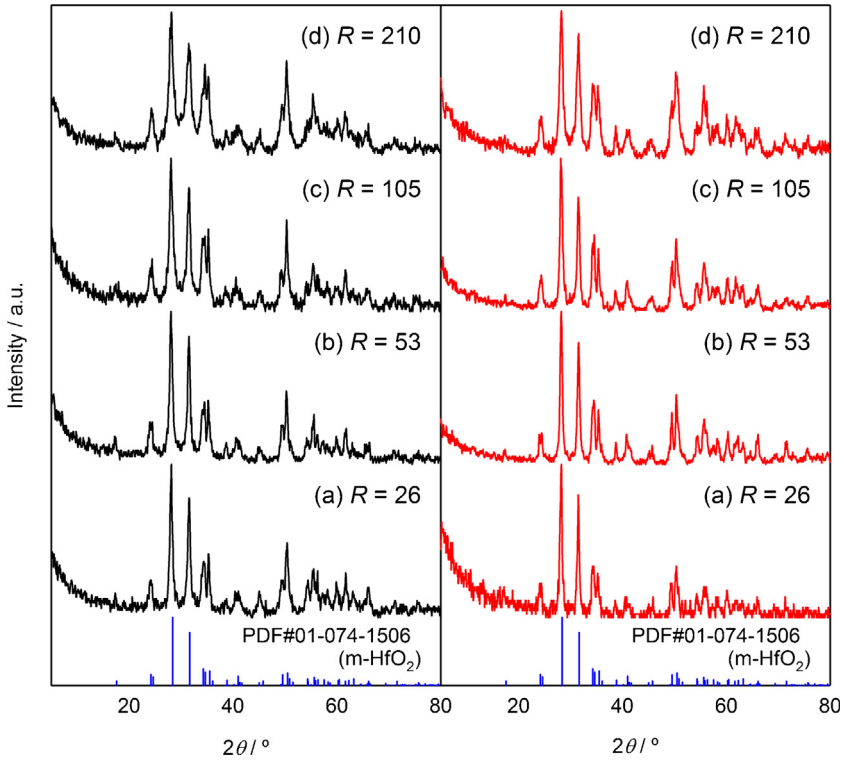

Fig. 1. X-ray diffraction patterns of HfO_x–rGO at four different *R* values: (a) 26, (b) 53, (c) 105, and (d) 210 before (left) and after (right) pyrolysis at *T* = 1273 K for 2 h under N_2.

radiation generated at 30 kV and 50 mA in the scan range of 5–80°, with a step size of 0.02°, at a scan rate of 2° min^{-1}. The chemical states of the catalysts were analyzed using an X-ray photoelectron spectrometer (PHI 5000 VersaProbe, ULVAC-PHI, Inc., Japan) with an Al-Kα X-ray source (1486.6 eV). The peak shift due to the surface charge was corrected using the binding energy of C 1 s at 284.8 eV. The morphology of the selected HfO_x–rGO catalyst was investigated using a field emission transmission electron microscope (JEM-2100F, JEOL, Japan).

2.3. ORR activity and selectivity measurements

RDE and RRDE voltammograms were obtained to evaluate the ORR activity and selectivity of the catalysts. The mixture of catalysts in a 5% w/w Nafion solution (510211, Sigma–Aldrich Co., U.S.) and isopropyl alcohol was sonicated for 1200 s then mixed using a planetary mixer (Mazerustar KK-250S, Kurabo Co., Japan) for 180 s to obtain a homogeneous catalyst ink. The mass fraction of the catalysts in the ink was 4.5% and the catalyst to Nafion mass ratio was 7:3 [24]. An aliquot (several mm^3) of the ink was dropped onto a glassy carbon (GC) disk (diameter: 4 mm)—platinum (Pt) ring (inner diameter: 5 mm; outer diameter: 7 mm) electrode (12613, BAS Co., Japan) and air-dried at 320 K for at least 600 s. The dropping and drying procedure was repeated until the GC electrode was coated with the desired mass of catalyst and Nafion, which was typically 0.4 mg; this value corresponded to a catalyst loading, m, of 2 mg cm^{-2}. Notably, the present catalysts require a large m to uniformly coat the GC surface owing to the high density. Prior to the treatment, the surface of the GC disk electrodes was polished with 1.0 and 0.05 μm alumina slurries, washed with water, and then dried at 320 K in air. A conventional three-electrode cell was used, and electrochemical measurements were performed in 0.1 mol dm^{-3} H_2SO_4 at room temperature. The catalyst-coated GC disk—Pt ring electrode, carbon rod (diameter: 5 mm, C-072591, Nilaco Co., Japan), and Ag/AgCl (3 mol dm^{-3} NaCl) electrode (RE-1B, BAS Co., Japan) were used as working, counter, and reference electrodes, respectively. The working electrode was set on a rotator (RRDE-3A, BAS Co., Japan). All working electrode potentials were referenced to the RHE. Using a potentiostat (Model 2323, BAS Co., Japan), the RDE and RRDE voltammograms were recorded by applying a disk potential, E_d, over the range of 0.11–1.26 V at a scan rate of 5 mV s^{-1} and a rotation speed of 1500 rpm after sequentially bubbling with O_2 and N_2 for 1800 s. The ring potential, E_r, was kept constant at 1.26 V to obtain the RRDE voltammograms. The ORR was assumed to be derived from the difference between the current obtained under N_2 (I_{dN}) and that obtained under O_2 (I_{dO}). Cyclic voltammograms (CVs) were acquired over the same E_d range of 0.11–1.26 V at a scan rate of 50 mV s^{-1} without rotation under N_2 to evaluate the double layer capacitance.

3. Results and discussion

3.1. Effect of R on crystal structure and chemical states of HfO_x–rGO

Fig. 1 shows the XRD patterns of HfO_x–rGO catalysts with four R values ranging from 26 to 210 before (left) and after (right) pyrolysis at a fixed T of 1273 K for 2 h under N_2 gas. 1273 K was the optimum T for both the ORR activity and selectivity (Supplementary Information, S1). All HfO_x–rGO catalysts exhibited a single monoclinic HfO_2 phase before pyrolysis, which was indicative of the hydrolysis of $HfCl_4$ owing to the hydrothermal treatment. There were no peaks at $2\theta = 10°$ of GO precursor (Supplementary information, S2) suggesting that the GO sheets were reduced by the hydrothermal treatment. Other groups also reported the disappearance of the GO-derived XRD peak by hydrothermal treatments [25,26]. The following pyrolysis at 1273 K did not alter the patterns, indicating the absence of impurities owing to unreacted precursors etc.

The surface chemical states of these catalysts were evaluated using XPS. In this study, C 1s spectra were not used as they include contributions from contaminants in the spectrometer. Hf 4f, O 1s and N 1s spectra before and after pyrolysis at T = 1273 K are shown in Fig. 2 with dashed and solid curves, respectively. It is well known that the Hf 4f level is split into the Hf $4f_{7/2}$ and Hf $4f_{5/2}$ sublevels by spin–orbit coupling; thus this peak is observed in the Hf 4f spectra as a doublet. When R was 26, the HfO_x–rGO catalyst showed a doublet at ~17.3 eV and ~19.0 eV before pyrolysis, which is typical

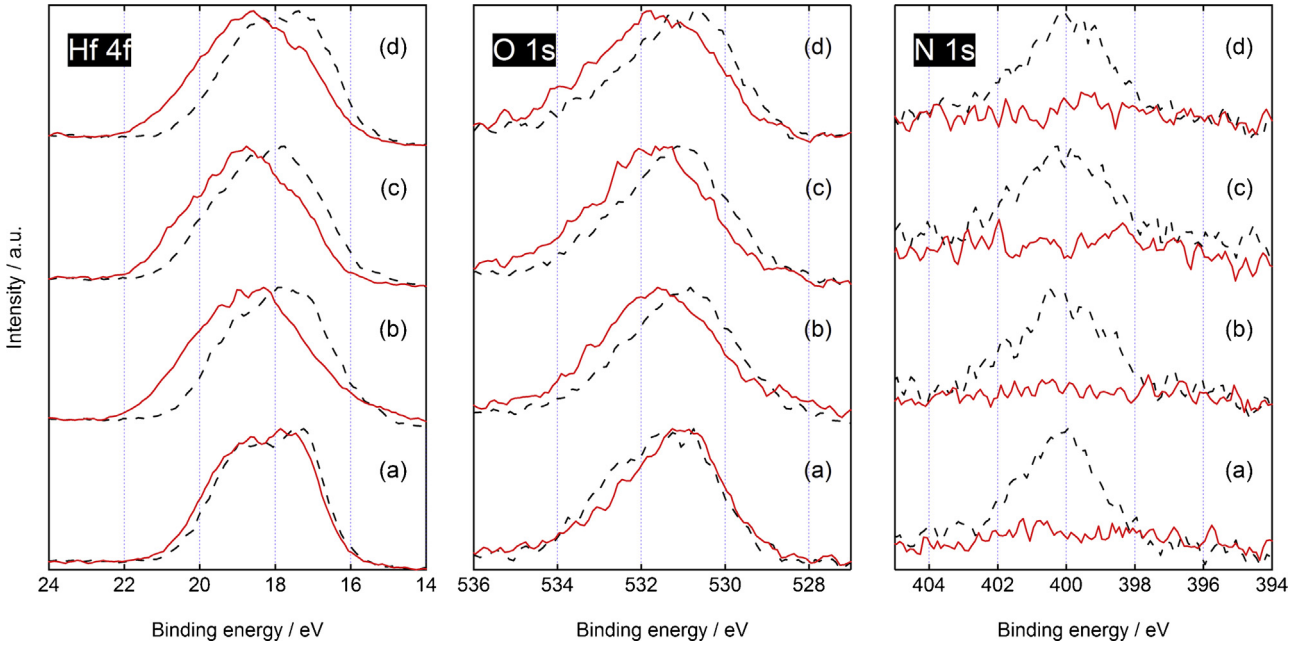

Fig. 2. (Left) Hf 4f, (center) O 1s and (right) N 1s spectra of HfO_x–rGO at four different R values: (a) 26, (b) 53, (c) 105, and (d) 210 before (dashed curves) and after (solid curves) pyrolysis at T = 1273 K for 2 h under N_2.

of Hf^{4+} in HfO_2 [27–29]. The Hf 4f spectrum did not significantly change after pyrolysis, as shown in the left part of Fig. 2 (a). In contrast, the Hf 4f peak shifted to a higher binding energy region after pyrolysis when $R = 53–210$, as shown in the left part of Fig. 2(b)–(d). Copel et al. reported that both Hf 4f and O 1s peaks shifted to higher binding energies by the incorporation of charged oxygen defects on HfO_2 in contact with metals created after pyrolysis [28]. The shift of both Hf 4f and O 1s peaks to higher binding energy regions after the incorporation of oxygen defects on HfO_2 has also been reported by Cho et al. [29]. Similarly, after pyrolysis when $R = 53–210$, charged oxygen defects could be produced at carbon/HfO_2 interface via a so-called carbothermal reduction, which is the reaction between carbon layers and HfO_2 to produce oxygen defects and some by-products, e.g., carbon dioxide [$HfO_2 + (1–0.5x)C \rightarrow HfO_x + 0.5(2–x)CO_2$]. Although some contributions from GO could be contaminated, O 1s spectra shown in the center of Fig. 2 also support this postulate that oxygen defects were incorporated at $R = 53–210$; the peaks shifted to higher binding energy regions by the pyrolysis whereas it didn't shift when $R = 26$. The amount of oxygen defects incorporated by pyrolysis were assumed to be the same when $R = 53–210$, because the corresponding Hf 4f spectra were nearly the same. The N 1s spectra shown in the right part of Fig. 2(a)–(d) were significantly altered by pyrolysis. The peaks at 398–402 eV, which were assigned to several nitrogen functionalities on rGO and/or carbon species originated from the L(+)-lysine precursor [30], disappeared after pyrolysis, indicating that nitrogen atoms from unreacted L(+)-lysine and/or those doped into carbon species after the hydrothermal treatment were removed by pyrolysis at 1273 K. Similar oxidation results, i.e., removal of all nitrogen atoms from the catalyst surface, have been reported for carbon-supported HfO_xN_y catalysts subjected to pyrolysis at 1323 K under a flow of mixed gas containing 5% H_2 and 95% Ar [31] and carbon-supported titanium oxynitride catalyst after pyrolysis at 1173 K under N_2 [32]. A brief summary of this subsection is as follows: a monoclinic HfO_2 phase was formed at any R after the hydrothermal treatment. After pyrolysis at $T = 1273$ K, a stoichiometric monoclinic-HfO_2 phase free from both nitrogen atoms and defects was synthesized when $R = 26$. Similar amounts of oxygen defects were incorporated into the HfO_2 phase at $53 \leq R \leq 210$.

3.2. Effect of R on ORR activity of HfO_x–rGO

The ORR activity was evaluated using RDE voltammograms. All data were corrected by subtracting the current under N_2 from that under O_2 to eliminate the capacitive contribution, which does not originate from ORR. Then the ORR current per unit mass of the catalyst, $i_{dO}–i_{dN}$, was used as a measure of activity. Fig. 3 shows the $i_{dO}–i_{dN}$ versus Ed curves of HfO_x–rGO catalysts at four R values ranging from 26 to 210 after pyrolysis at $T = 1273$ K. These catalysts showed no ORR activity at $E_d > 0.4$ V before pyrolysis (Supplementary Information, S1), indicating that pyrolysis was necessary to create active sites. Three HfO_x–rGO catalysts whose $R \geq 53$ showed $i_{dO}–i_{dN}$ at around $E_d = \sim 0.9$ V whereas more than 0.1 V lower onset potential was observed for $R = 26$, suggesting that the quality of the active sites was almost the same at $53 \leq R \leq 210$. This trend was in good agreement with the amount of oxygen defects obtained from XPS analyses (Fig. 2), suggesting that oxygen defects formed active sites. However, the number of active site represented by $|i_{dO}–i_{dN}|$ at lower E_d was clearly different and depending on R; it increased as R increased up to 105, but decreased with a further increase of R to 210. The trend was the same when geometrical current density was used instead of mass activity (Supplementary Information, S3). The CVs obtained under N_2 are shown in Fig. 4 to compare the double layer capacitance. Except for $R = 26$, the shape of the CVs was typical of carbon materials with graphitic structures and presented a quinone/hydroquinone redox couple at $E_d = \sim 0.6$ V [33]. The double layer capacitance monotonically increased with increasing R values in the range of 53–210, indicating that L(+)-lysine increased the surface area via two possible routes; the one is that L(+)-lysine acted as a carbon source by itself and the other is that decomposition of L(+)-lysine increased the surface area of rGO. The CV shape was clearly different when R was 26, suggesting that the amount of L(+)-lysine was too small to form a graphitic structure. The morphology of the catalyst that showed the highest activity was investigated using FE-TEM. Three different phases were observed, as shown in Fig. 5, which is a FE-TEM image of HfO_x–rGO whose $R = 105$ after pyrolysis at $T = 1273$ K. A black particle displayed clear lattice fringes (0.28 nm), which was assigned to the (111) plane of monoclinic HfO_2. The other two phases, dark grey amorphous parts in contact with the black particle and light-

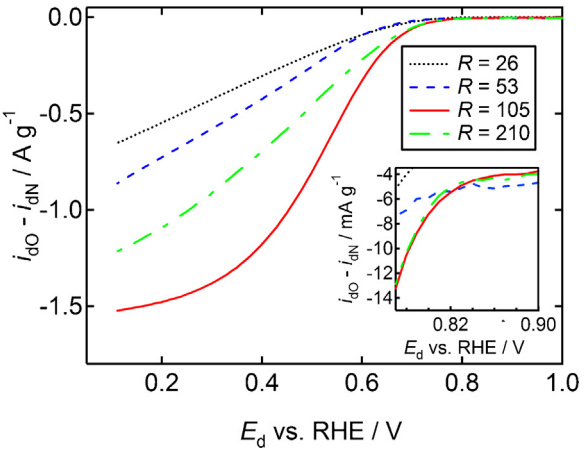

Fig. 3. ORR mass activity versus disk potential [($i_{dO}–i_{dN}$)–E_d] curves of HfO_x–rGO for four different R values: (a) 26, (b) 53, (c) 105 and (d) 210 after pyrolysis at $T = 1273$ K for 2 h under N_2. Scans were performed under N_2 and O_2, with a rotation speed of 1500 rpm, at a scan rate of 5 mV s^{-1}, in 0.1 mol dm^{-3} H_2SO_4 solution.

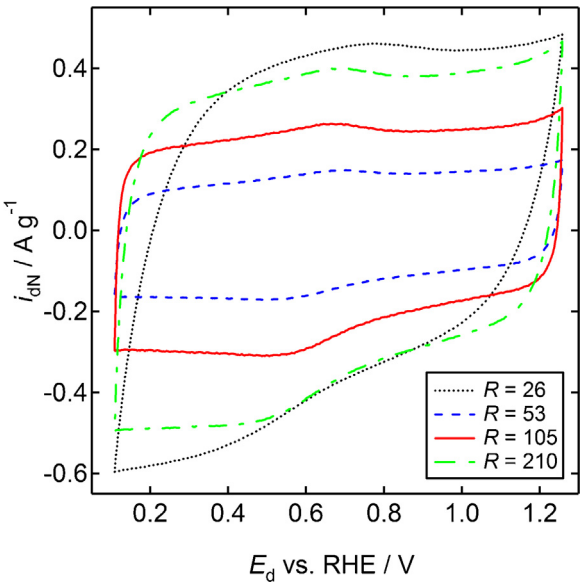

Fig. 4. Cyclic voltammograms of HfO_x–rGO at four different R values: (a) 26, (b) 53, (c) 105, and (d) 210 after pyrolysis at $T = 1273$ K for 2 h under N_2. Scans were performed under N_2 at a scan rate of 50 mV s^{-1} in 0.1 mol dm^{-3} H_2SO_4 solution.

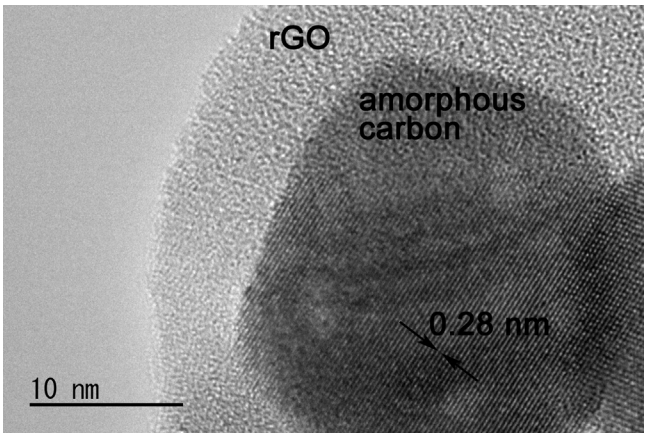

Fig. 5. A field emission-transmission electron microscopy image of HfO_x–rGO whose $R = 105$ after pyrolysis at $T = 1273$ K for 2 h under N_2.

grey sheets exhibited no lattice fringes. The dark grey amorphous parts are clearly different from light-grey sheets. Xu et al. reported that L(+)-lysine carbonized during the hydrothermal treatment of $TiCl_4$ and L(+)-lysine in water at 453 K for 12 h [21]. Although the hydrothermal route was modified from their study by adding GO powders and changing $TiCl_4$ to $HfCl_4$, the hydrothermal temperature and time used in this study are identical to those which they used. These results in combination with the CVs (Fig. 4) suggested that dark-grey colored amorphous carbon species originated from L(+)-lysine connected the black HfO_2 particle with the light-grey rGO sheets.

3.3. Discussion of ORR active site formation and role of L(+)-lysine

The XPS analyses revealed that nitrogen atoms in the L(+)-lysine precursor were completely removed by pyrolysis at 1273 K at any *R*. In acidic media, nitrogen-doped carbon catalysts synthesized in the absence of iron/cobalt species can show ORR activity at E_d below 0.8 V [34], lower than that of PGM and other non-PGM catalysts with iron/cobalt species. The situation is different in alkaline counterparts: iron/cobalt-free nitrogen-doped carbon catalysts can show ORR activity comparable to that of PGM catalysts [35] and even carbons free from both nitrogen and iron/cobalt atoms show activity [26,36]. Although the present HfO_x–rGO catalysts after pyrolysis were free from nitrogen atoms and the activity was evaluated in acidic media, some contributions from rGO supports cannot be excluded at $E_d < 0.8$ V. We focused on the properties of HfO_x particles to clarify the active sites that determined onset potential of above 0.8 V. The CVs and FE-TEM image demonstrated that L(+)-lysine worked as a carbon source when $R = 53$–210 and the amount of deposited carbon increased with increasing *R*. The deposited carbon played two important roles in forming and evaluating ORR active sites, as illustrated in Fig. 6. When *R* was 26, the amount of L(+)-lysine was insufficient to form carbon layers which would provide an electronic path, resulting in a poor ORR current. Because HfO_2 is an insulator, the active surface area should be restricted to the point where it contacts conductive supports, as indicated by the arrow in Fig. 6(i). The surface of the particle was stoichiometric HfO_2 free from defects. When *R* was greater than 26, the amount of L(+)-lysine was sufficient to form carbon layers that produced both electronic paths and ORR-active oxygen defects by the so-called carbothermal reduction. Therefore, both the activity level evaluated by the onset potential and the amount of oxygen defects were almost the same at $53 \leq R \leq 210$. In the *R* range, the number of electrons transferred per unit oxygen molecule, *n*, at $E_d = 0.6$ V varied a little from 3.5 to 3.7, suggesting that ORR proceeded via the similar mechanism; mostly 4-electron reaction in which oxygen molecules were directly reduced to water ($O_2 + 4H^+ + 4e^- \rightarrow 2H_2O$). However, evaluation of all the active sites on the insulating oxide particles was difficult when *R* was too small or large. The number of evaluated active sites represented by the ORR mass activity, $|i_{dO} - i_{dN}|$ at lower E_d was maximized when $R = 105$. Because ORR is an electrocatalytic reaction, all electrons, protons, and oxygen molecules should be supplied to the active sites. The CV results shown in Fig. 4 indicate that the amount of deposited carbon from L(+)-lysine increased with increasing *R* to provide electronic paths for active sites, but transport of oxygen molecules should be restricted with increasing thicknesses of the deposited carbon layers, thereby resulting in the decrease of $|i_{dO} - i_{dN}|$. From these results, coating the oxide catalyst particles with a conductive layer was necessary, as expected. However, too many carbon layers hindered the accurate evaluation of the number of ORR active sites and thus the optimization of the carbon source content was necessary. The optimization can be done only when the source of oxide and carbon were different, which differed from the case of oxy-metal phthalocyanine. L(+)-lysine was found to serve as an

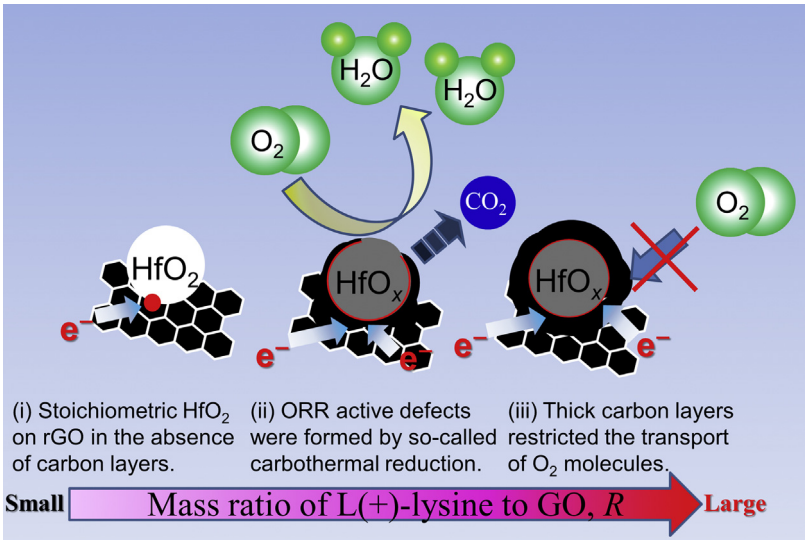

Fig. 6. Schematic image of HfO_x–rGO catalysts with various *R*.

excellent carbon source for this purpose without forming nitrogen-doped carbon species that make discussion difficult. By coating the nitrogen-free HfO_x particles with L(+)-lysine-derived carbon layers at the optimum content, an onset potential of ca. 0.9 V was obtained in this study. This value is greater than that of other hafnium oxide-based catalysts which have been doped with nitrogen atoms [17,19,24]. This is the first study to show such high activity from nitrogen-free HfO_x phases with oxygen defects. However, Fig. 5 displays that the amorphous carbon species did not cover all the HfO_x surface, suggesting the needs in modification of the synthesis route to increase the coverage and resulting conductivity. By coating all the catalyst surface with thin carbon layers, the number of active sites could be increased further. At E_d = 0.8 V, the HfO_x–rGO obtained in this study showed ~7 mA g^{-1} of mass activity, which is about three times higher than that obtained from HfO_xN_y–rGO which was synthesized in the absence of carbon sources [19]. Coating the surface of these nitrogen-doped oxide catalysts with thin carbon layers will constitute the next research topic.

4. Conclusions

Nitrogen-free HfO_x–rGO catalysts were synthesized via a modified hydrothermal route, followed by pyrolysis under N_2. FE-TEM analyses revealed that amorphous carbon layers connected HfO_x nanoparticles with rGO sheets by adding sufficient amounts of L(+)-lysine to the precursor dispersion. The double layer capacitance from the CVs monotonically increased with increasing R in the range of 53–210, indicating that the carbon layers were conductive and originated from L(+)-lysine. The nitrogen-free carbon layers played two important roles for enhancing and evaluating ORR activity: (i) creating the ORR-active oxygen defect sites by pyrolysis and (ii) increasing the number of active sites that could be evaluated. The mechanism for (i) was proposed to occur via carbothermal reduction. The optimum R for (ii) was 105, owing to the increase in conductivity and decrease in oxygen diffusivity. L(+)-lysine was found to be an excellent source of carbon, which enhanced the onset potential to 0.9 V, and aided in the evaluation of the number of ORR active defect sites after the optimization of R.

Acknowledgments

We thank Mr. Yusei Tsushima for his help with obtaining FE-TEM images. This work was partially supported by a Grant-in-Aid for Scientific Research (C), 26420132, from the Ministry of Education, Culture, Sports, Science, and Technology (MEXT) in Japan and a research grant from Takahashi Industrial and Economic Research Foundation in Japan. The XPS analyses were supported by Nanotechnology Platform, 12024046 of the MEXT in Japan.

Appendix A. Supplementary data

Supplementary data associated with this article can be found, in the online version, at http://dx.doi.org/10.1016/j.electacta.2015.10.184.

References

[1] F. Jaouen, Non-Noble Metal Fuel Cells Catalysts, in: Z. Chen, J.P. Dodelet, J. Zhang (Eds.), Wiley-VCH, Weinheim, 2014, pp. 29.
[2] F. Jaouen, J. Herranz, M. Lefèvre, J.P. Dodelet, U.I. Kramm, I. Herrmann, P. Bogdanoff, J. Maruyama, T. Nagaoka, A. Garsuch, J.R. Dahn, T. Olson, S. Pylypenko, P. Atanassov, E.A. Ustinov, Cross-Laboratory Experimental Study of Non-Noble-Metal Electrocatalysts for the Oxygen Reduction Reaction, ACS Appl. Mater. Interfaces 1 (2009) 1623.
[3] X. Wang, J.S. Lee, Q. Zhu, J. Liu, Y. Wang, S. Dai, Ammonia-Treated Ordered Mesoporous Carbons as Catalytic Materials for Oxygen Reduction Reaction, Chem. Mater. 22 (2010) 2178.
[4] Y. Li, W. Zhou, H. Wang, L. Xie, Y. Liang, F. Wei, J.C. Idrobo, S.J. Pennycook, H. Dai, An Oxygen Reduction Electrocatalyst Based on Carbon Nanotube–Graphene Complexes, Nat. Nanotechnol. 7 (2012) 394.
[5] W. Wei, H. Liang, K. Parvez, X. Zhuang, X. Feng, K. Müllen, Nitrogen-Doped Carbon Nanosheets with Size-Defined Mesopores as Highly Efficient Metal-Free Catalyst for the Oxygen Reduction Reaction, Angew. Chem. Int. Ed. 126 (2014) 1596.
[6] J. Shui, M. Wang, F. Du, L. Dai, N-doped Carbon Nanomaterials are Durable Catalysts for Oxygen Reduction Reaction in Acidic Fuel Cells, Sci. Adv. 1 (2015) e1400129.
[7] M. Lefevre, E. Proietti, F. Jaouen, J.P. Dodelet, Iron-Based Catalysts with Improved Oxygen Reduction Activity in Polymer Electrolyte Fuel Cells, Science 324 (2009) 71.
[8] E. Proietti, F. Jaouen, M. Lefevre, N. Larouche, J. Tian, J. Herranz, J.P. Dodelet, Iron-Based Cathode Catalyst with Enhanced Power Density in Polymer Electrolyte Membrane Fuel Cells, Nat. Commun. 2 (2011) 416.
[9] G. Wu, K.L. More, C.M. Johnston, P. Zelenay, High-Performance Electrocatalysts for Oxygen Reduction Derived from Polyaniline, Iron, and Cobalt, Science 332 (2011) 443.
[10] J. Yin, Y. Qiu, J. Yu, Onion-like Graphitic Nanoshell Structured Fe–N/C Nanofibers Derived from Electrospinning for Oxygen Reduction Reaction in Acid Media, Electrochem. Commun 30 (2013) 1.
[11] H.J. Zhang, H. Li, X. Li, S. Zheng, B. Zhao, J. Yang, Highly Active Electrocatalyst for Oxygen Reduction Reaction from Pyrolyzing Carbon-Supported Iron Tetraethylenepentamine Complex, Appl. Catal. B: Environmental 160 (2014) 676.
[12] V. Goellner, C. Baldizzone, A. Schuppert, M.T. Sougrati, K. Mayrhofer, F. Jaouen, Degradation of Fe/N/C Catalysts Upon High Polarization in Acid Medium, Phys. Chem. Chem. Phys. 16 (2014) 18454.
[13] S. Doi, A. Ishihara, S. Mitsushima, N. Kamiya, K. Ota, Zirconium-Based Compounds for Cathode of Polymer Electrolyte Fuel Cell, J. Electrochem. Soc. 154 (2007) B362.
[14] J.H. Kim, A. Ishihara, S. Mitsushima, N. Kamiya, K. Ota, Catalytic Activity of Titanium Oxide for Oxygen Reduction Reaction as a Non-Platinum Catalyst for PEFC, Electrochim. Acta 52 (2007) 2492.
[15] A. Ishihara, S. Doi, S. Mitsushima, K. Ota, Tantalum (Oxy) nitrides Prepared Using Reactive Sputtering for New Nonplatinum Cathodes of Polymer Electrolyte Fuel Cell, Electrochim. Acta 53 (2008) 5442.
[16] M. Chisaka, T. Iijima, T. Yaguchi, Y. Sakurai, Carbon-Supported Hafnium Oxynitride as Cathode Catalyst for Polymer Electrolyte Membrane Fuel Cells, Electrochim. Acta 56 (2011) 4581.
[17] M. Chisaka, Y. Suzuki, T. Iijima, Y. Sakurai, Effect of Synthesis Route on Oxygen Reduction Reaction Activity of Carbon-Supported Hafnium Oxynitride in Acid Media, J. Phys. Chem. C 115 (2011) 20610.
[18] J.Y. Kim, T.K. Oh, Y. Shin, J. Bonnett, K. Scott Weil, A Novel Non-Platinum Group Electrocatalyst for PEM Fuel Cell Application, Int. J. Hydrogen Energy 36 (2011) 4557.
[19] M. Chisaka, H. Sasaki, H. Muramoto, Monoclinic Hafnium Oxynitride Supported on Reduced Graphene Oxide to Catalyse the Oxygen Reduction Reaction in Acidic Media, Phys. Chem. Chem. Phys. 16 (2014) 20415.
[20] A. Ishihara, M. Chisaka, Y. Ohgi, K. Matsuzawa, S. Mitsushima, K. Ota, Synthesis of Nano-TaOx Oxygen Reduction Reaction Catalysts on Multi-Walled Carbon Nanotubes Connected via a Decomposition of Oxy-tantalum Phthalocyanine, Phys. Chem. Chem. Phys 17 (2015) 7643.
[21] D.H. Wang, L. Jia, X.L. Wu, L.Q. Lu, A.W. Xu, One-Step Hydrothermal Synthesis of N-Doped TiO_2/C Nanocomposites with High Visible Light Photocatalytic Activity, Nanoscale 4 (2012) 576.
[22] U.S. Geological Survey, Metal Prices in the United States Through 2010 http://pubs.usgs.gov/sir/2012/5188/sir2012-5188 pdf (accessed 08.09.15).
[23] U.S. Geological Survey, Mineral Commodity Summaries 2010, http://minerals.usgs.gov/minerals/pubs/mcs/2010/mcs2010 pdf (accessed 08.09.15).
[24] M. Chisaka, H. Muramoto, Suppression and Evaluation of Hydrogen Peroxide Formation on Carbon-Supported Hafnium Oxynitride, ECS Electrochem. Lett. 3 (2014) F1.
[25] L. Liu, S. Zhang, Effective Solvothermal Deoxidization of Graphene Oxide Using Solid Sulphur as a Reducing Agent, J. Mater. Chem. 22 (2012) 14385.
[26] W.I. Hayes, P. Joseph, M.Z. Mughal, P. Papakonstantinou, Production of Reduced Graphene Oxide via Hydrothermal Reduction in an Aqueous Sulphuric Acid Suspension and its Electrochemical Behaviour, J. Solid State Electrochem. 19 (2015) 361.
[27] S. Hofmann, J.M. Sanz, Quantitative XPS analysis of the Surface Layer of Anodic Oxides Obtained during Depth Profiling by Sputtering with 3 keV Ar^+ ions, J. Trace Microprobe Technol. 1 (1982) 213.
[28] M. Copel, R.P. Pezzi, D. Neumayer, P. Jamison, Reduction of Hafnium Oxide and Hafnium Silicate by Rhenium and Platinum, Appl. Phys. Lett. 88 (2006) 072914.
[29] D.Y. Cho, C.H. Min, J. Kim, S.J. Oh, M.G. Kim, Bond nature of oxygen-deficient HfO_2/Si (1 0 0) film, Appl. Phys. Lett. 89 (2006) 253510.
[30] J.R. Pels, F. Kapteijn, J.A. Moulijn, Q. Zhu, K.M. Thomas, Evolution of Nitrogen Functionalities in Carbonaceous Materials During Pyrolysis, Carbon 33 (1995) 1641.
[31] M. Chisaka, Y. Suzuki, T. Iijima, Y. Ishihara, R. Inada, Y. Sakurai, Active Sites for Oxygen Reduction Reaction and the Reaction Mechanism in Carbon-Supported Hafnium Oxynitride, ECS Electrochem. Lett. 1 (2012) F4.

[32] M. Chisaka, Y. Ando, H. Muramoto, Facile Combustion Synthesis of Carbon-Supported Titanium Oxynitride to Catalyse Oxygen Reduction Reaction in Acidic Media, Electrochim. Acta 183 (2016) 100–106.
[33] H. Gomathi, G. Prabhakara Rao, Chemical and Electrochemical Modification of the Glassy Carbon Surface with Quinhydrone, J. Electroanal. Chem. 190 (1985) 85.
[34] J.P. Dodelet, The Controversial Role of the Metal in Fe-or Co-based Electrocatalysts for the Oxygen Reduction Reaction in Acid Medium, in: M. Shao (Ed.), Electrocatalysis in Fuel Cells: A Non- and Low-Platinum Approach, Springer, London, 2013, pp. 271.
[35] R. Liu, D. Wu, X. Feng, K. Müllen, Nitrogen-Doped Ordered Mesoporous Graphitic Arrays with High Electrocatalytic Activity for Oxygen Reduction, Angew. Chem. 122 (2010) 2619.
[36] N. Soin, S.S. Roy, S. Sharma, T. Thundat, J.A. McLaughlin, Electrochemical and Oxygen Reduction Properties of Pristine and Nitrogen-Doped Few Layered Graphene Nanoflakes (FLGs), J. Solid State Electrochem. 17 (2013) 2139.